Electronic devices based on purified carbon nanotubes grown by high-pressure decomposition of carbon monoxide

DANVERS E. JOHNSTON, MOHAMMAD F. ISLAM*, ARJUN G. YODH AND ALAN T. JOHNSON*

Department of Physics and Astronomy, University of Pennsylvania, Philadelphia, Pennsylvania 19104, USA

*e-mail: islam@physics.upenn.edu; cjohnson@physics.upenn.edu

Published online: 17 July 2005; doi:10.1038/nmat1427

The excellent properties of transistors, wires and sensors made from single-walled carbon nanotubes (SWNTs) make them promising candidates for use in advanced nanoelectronic systems[1]. Gas-phase growth procedures such as the high-pressure decomposition of carbon monoxide (HiPCO) method[2,3] yield large quantities of small-diameter semiconducting SWNTs, which are ideal for use in nanoelectronic circuits. As-grown HiPCO material, however, commonly contains a large fraction of carbonaceous impurities that degrade the properties of SWNT devices[4]. Here we demonstrate a purification, deposition and fabrication process that yields devices consisting of metallic and semiconducting nanotubes with electronic characteristics vastly superior to those of circuits made from raw HiPCO. Source–drain current measurements on the circuits as a function of temperature and backgate voltage are used to quantify the energy gap of semiconducting nanotubes in a field-effect transistor geometry. This work demonstrates significant progress towards the goal of producing complex integrated circuits from bulk-grown SWNT material.

To date, most work on nanotube electronics has relied on SWNTs grown directly onto substrates by chemical vapour deposition (CVD)[5–7]. CVD-grown SWNTs have clean sidewalls, enabling high-quality electrical contact to metal electrodes[8,9], and they hold promise for accurate placement in integrated circuits using patterned catalysts. However, the use of such material for integrated devices is made difficult by lack of control over whether individual SWNTs are metallic or semiconducting. Moreover, semiconducting SWNTs grown by CVD are typically of large diameter (2–4 nm), leading to an energy bandgap much less than 1 eV. This makes them incompatible with designs for nanoelectronic logic gates consisting of SWNT transistors with high ON/OFF ratios.

Gas-phase growth procedures such as the HiPCO method routinely yield large quantities of SWNTs with diameters less than 1 nm, and they are being scaled to produce industrial quantities. Growth conditions producing semiconducting SWNTs with a narrow distribution of wrapping vector have been reported[10], and dispersion of HiPCO material as isolated nanotubes has been achieved using amphiphilic molecules[11–14], enabling schemes for sorting SWNTs by length[15,16], diameter[13], or metallicity[17,18]. Finally, dispersed SWNTs have been controllably deposited onto patterned substrates, exploiting specific interactions between the adsorbed amphiphilic molecules and surface monolayers[19,20].

A major challenge to realizing the potential of HiPCO material for devices is that it usually contains a significant quantity of carbonaceous impurities known to have deleterious effects on the properties of single-nanotube devices. Standard acid-based or oxidation-based purification approaches damage SWNTs and sharply degrade their electronic characteristics (S. Paulson, H. Wadhar, C. Staii, and A.T.J. to be published). In addition, one must remove the amphiphilic molecules after depositing SWNTs onto substrates because residual surfactant on the SWNT leads to poor contact to the electrodes.

Details of the new purification process are provided in the Methods section. Briefly, as-grown HiPCO material is purified by heating in wet air in the presence of H_2O_2, gentle acid treatment, magnetic fractionation[21,22], and vacuum annealing. The dominant impurities in as-grown HiPCO are catalyst particles and non-SWNT carbon phases. Thermogravimetric analysis and wide-angle X-ray scattering measurements indicate that the impurity content is more than 50 wt% in as-grown HiPCO and less than 5 wt% after purification. Based on this measured impurity content and the measured sample mass after purification, the purification process recovers close to 90% of the SWNT content of the HiPCO. The material to be tested (either raw or purified HiPCO) is dispersed in water using sodium dodecyl benzene sulfonate (NaDDBS)[11] and deposited onto degenerately doped oxidized (400 nm SiO_2) silicon wafers. Before deposition, the SiO_2 surface is functionalized with a 3-aminopropyl triethoxysilane (APTS) monolayer, and SWNTs are deposited by briefly dipping the chip in the SWNT-NaDDBS suspension. The sample is rinsed in deionized water, blown dry, and heated in air at 200 °C for 12 h. This last step removes a large fraction of the residual surfactant as shown by a systematic ~2 nm decrease of the nanotube diameter as measured by atomic force microscopy (AFM). This treatment also vaporizes the APTS monolayer from the bulk of the silicon substrate.

Figure 1a is an AFM image of individual SWNTs and small nanotube bundles after deposition from solution and surfactant removal. Cr/Au source and drain electrodes separated by 400 nm are fabricated with electron-beam lithography without alignment, followed by thermal evaporation and liftoff (Fig. 1b,c). The electrode density is chosen such that ~50% of the electrode pairs

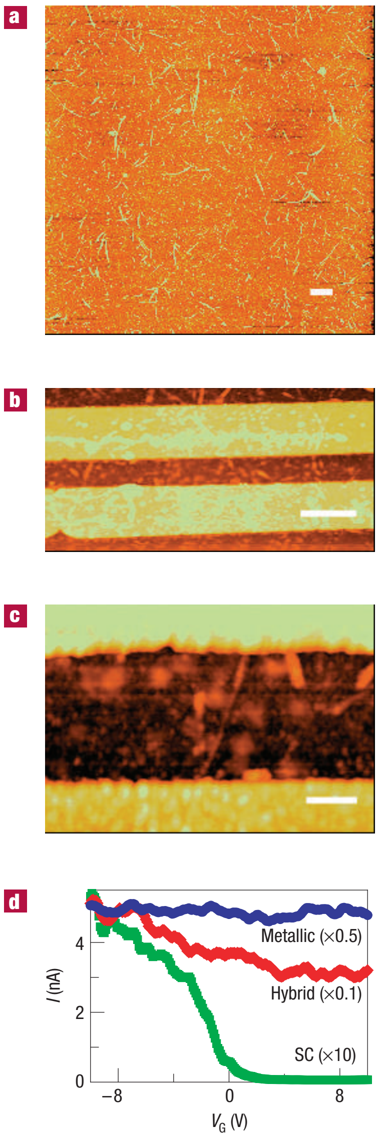

Figure 1 AFM images of devices made from purified HiPCO material. a, SiO_2 surface with individual SWNTs and small bundles after deposition from solution and surfactant removal (scale bar 1 μm). **b**, Cr/Au electrodes contacting SWNT material (scale bar 1 μm). **c**, High-resolution scan of a bundle 4 nm in diameter with source and drain electrodes along the top and bottom (scale bar 200 nm). **d**, Three categories of I–V_g behaviour are observed. The bias voltage is 10 mV.

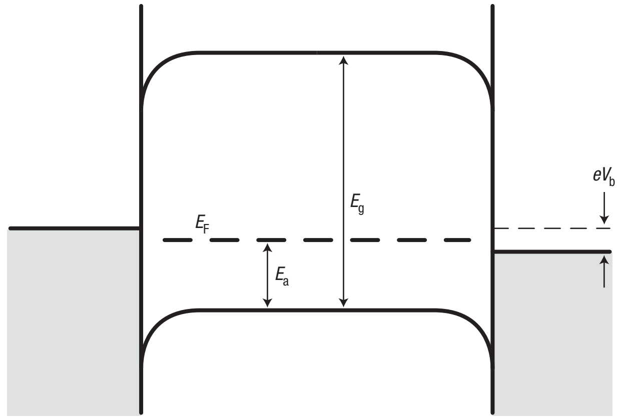

Figure 2 Model of device energy bands. Schottky barriers form where metal leads contact a semiconducting SWNT with energy gap E_g and applied bias voltage V_b. The Schottky barriers are asymmetric, so holes conduct more readily than electrons. Carriers tunnel through the Schottky barriers, so transport is characterized by an activation energy E_a, given by the difference between the Fermi energy E_F and the edge of the nearest energy band of the SWNT (here, the valence band).

conduct, typically contacting one SWNT or one small bundle. The degenerately doped silicon is used as a back gate electrode in a field-effect transistor (FET) geometry.

The source–drain current I is measured in ambient conditions for different values of the bias voltage V_b and gate voltage V_g. The behaviour of the I–V_g curve at low voltage bias (typically $V_b = 10$–100 mV) is used to categorize each sample as metallic (M), semiconducting (SC), or hybrid (H). Metallic samples have a relatively low source–drain resistance and I shows little or no gate response; we conclude that these samples consist of a single metallic SWNT or a bundle where only metallic SWNTs are contacted. Semiconducting samples exhibit a high ON/OFF ratio, with very large resistance in the OFF state. We presume that conduction occurs through a single semiconducting SWNT or a bundle where current is carried only by semiconducting nanotubes. Hybrid samples exhibit a small ON/OFF ratio of roughly 2–4. We attribute this behaviour to conduction by metallic and semiconducting SWNTs in parallel. Figure 1d shows examples of these three observed behaviours.

The quality of the purification process was tested by comparing circuits made using as-grown and purified samples from the same HiPCO batch. The fraction of conducting samples was ~25% (4/16 for raw and 7/30 for purified material) for both fabrication runs. Quoted resistance values for SC samples are for the 'ON' state ($V_g = -10$ V). M and SC circuits made from raw HiPCO had source–drain resistances near 1 GΩ, whereas for purified material we measured a median resistance of 4 MΩ for M/H samples; no SC samples were observed in this first trial. Purification thus leads to a decrease in sample resistance by a factor of more than 200. The electrical transport properties of 29 additional samples made from purified material were then measured and classified. Twenty-two samples were M/H with a median resistance of 500 kΩ. Seven samples were SC with a median resistance of 10 MΩ. These should be compared with typical resistances of 15 and 100 kΩ for M and SC circuits made in our laboratory with CVD-grown SWNTs. The typical ON/OFF ratio of SC devices was 300, with the highest exceeding 5,000. Six of the SC samples exhibited p-type gate behaviour similar to FETs made from CVD-grown SWNTs; one SC device had an ambipolar gate response, with both hole and electron conduction (Fig. 3a). Supplementary Table S1 is a complete listing of observed sample resistances.

The observed fraction of SC samples (24%) is consistent with HiPCO material having random chirality (that is, 2/3 semiconducting SWNTs and 1/3 metallic). If we assume that small SWNT bundles (2–4 nm in diameter as measured by AFM, as seen in Fig. 1a) show SC behaviour only if all of the 3–4 SWNTs on the bundle exterior contacted by the electrodes are semiconducting[23], then we expect 20–30% of samples to be SC, in satisfactory agreement with the data. However, more single-tube circuits must be measured to precisely quantify the distribution of metallic and semiconducting SWNTs produced by the HiPCO process.

Three sources increase the resistance in SWNT circuits above the quantum limit of $h/4e^2 \approx 6.4$ kΩ, where h is Planck's constant and e the electron charge. Contaminants on the SWNT sidewall increase the contact resistance by acting as tunnel barriers at the electrodes or causing poor wetting of the electrode metallization.

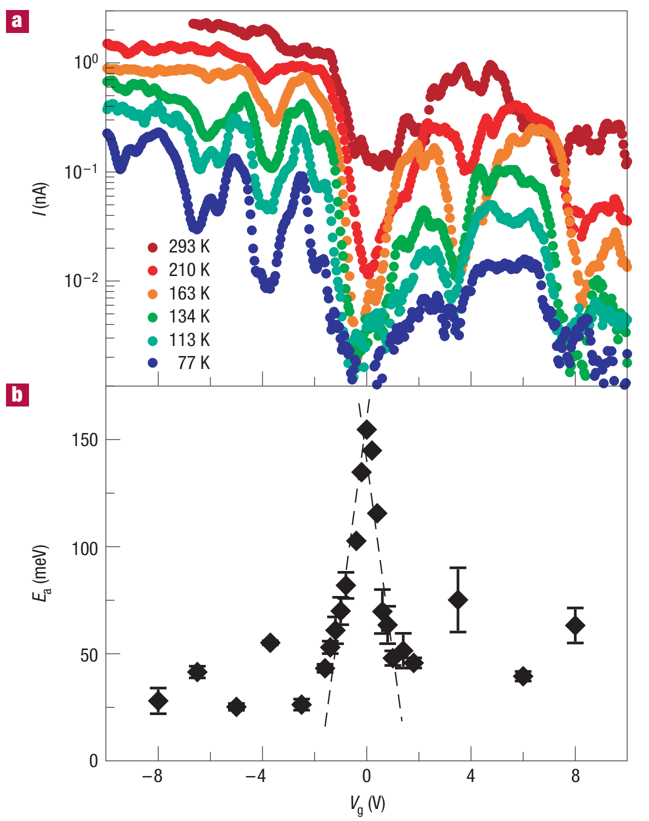

Figure 3 ***I*–*V*$_g$ characteristics for device I. a**, $I(V_g)$ at $V_b = 100$ mV for temperatures 77–300 K. **b**, Thermal activation energy E_a as a function of V_g. The peak in E_a corresponds to Fermi energy alignment at the midgap. Because the maximum of E_a is 150 meV, the energy gap is found to be 300 meV. The lever arm $\alpha \approx 0.08$ is inferred from the slope of a linear fit to E_a in the gap region. Oscillations in E_a outside the gap region are due to single-electron charging. Error bars for E_a are determined from a fit to the data using an Arrhenius plot (see inset to Fig. 4b).

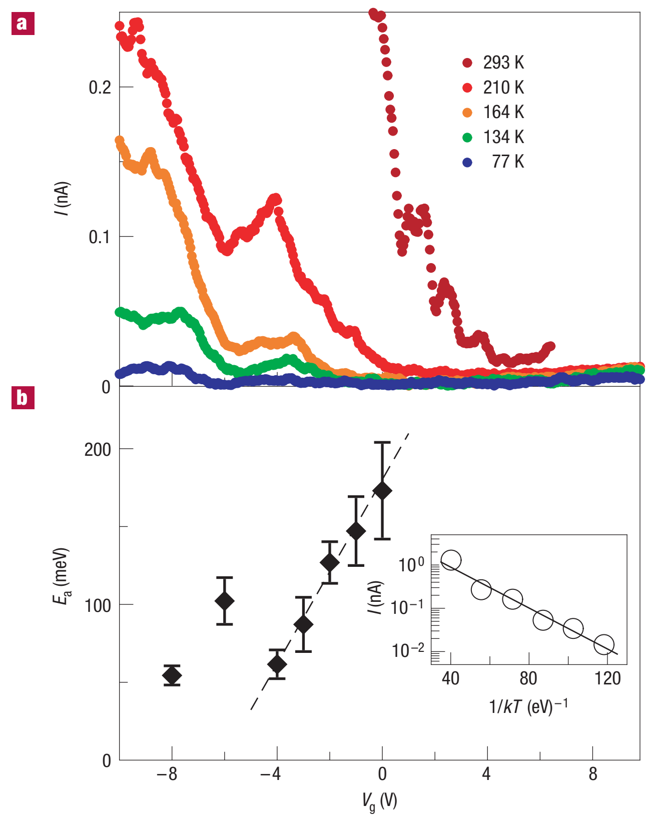

Figure 4 ***I*–*V*$_g$ characteristics for device II. a**, Temperature dependence of $I(V_g)$ with $V_b = 100$ mV. **b**, Activation energy E_a as a function of gate voltage. From the maximum value of E_a we find that the energy gap $E_g \geq 400$ mV. The lever arm for this sample is $\alpha \approx 0.03$. Oscillations in $I(V_g)$ and $E_a(V_g)$ for $V_g < -4$ V are due to single-electron charging effects. Inset: Arrhenius plot used to find the activation energy and its uncertainty for $V_g = -8$ V.

Schottky barriers form at the contacts to semiconducting (but not metallic) SWNTs, with minimum (tunnel) resistance near 100 kΩ (refs 24,25). Finally, electron backscattering along the length of the SWNT contributes to resistance. The carrier mean-free path for HiPCO is unknown but it can be several micrometres for clean metallic and semiconducting[26] SWNTs grown by CVD.

The high, nearly equal, resistances observed for M and SC devices from as-grown HiPCO indicate that in these samples sidewall contamination is the dominant source of resistance. The new purification process reduces the resistance of both types of sample by a factor of several hundred or more. Despite this improvement, devices from purified HiPCO have resistances significantly larger than those produced from CVD SWNTs. Further experiments will be needed to determine whether this is due to residual contamination that can be removed by an optimized purification process or a larger defect density in purified HiPCO material compared to CVD-grown SWNTs.

Temperature-dependent measurements of SC circuits made from purified material are consistent with thermally activated transport, with an activation energy E_a that varies with gate voltage (that is, $I(V_g, T) \propto e^{-E_a(V_g)/k_B T}$, where k_B is Boltzmann's constant). We understand this effect in the following way. Schottky barriers form at the contacts to nanotube FETs[24,25] (Fig. 2). Energy-band pinning in such devices is commonly asymmetric, so holes conduct more readily than electrons[27]. Electron conduction is typically still measurable in large-diameter (small-energy-bandgap) SWNTs, leading to ambipolar $I(V_g)$ characteristics (Fig. 3). In contrast, small-diameter (large-bandgap) SWNTs typically show p-type conduction, with electron conduction suppressed below measurement sensitivity (Fig. 4). As described below, the data agree with a model where the Schottky barrier acts as a tunnel barrier with different, temperature-independent transparencies for the two carrier types. When V_g is set so the Fermi energy E_F lies in the bandgap, transport occurs with an activation energy given by $E_a = |E_F - E_{band}|$, where E_{band} is the edge of the energy band (valence or conduction) closest to E_F; the activation energy is therefore expected to vary linearly with V_g, reaching a maximum of half the energy bandgap when E_F is situated at the midgap.

We see precisely this behaviour for the ambipolar sample, device I. Figure 3 shows the temperature dependence of $I(V_g)$ for this sample, the bundle 4 nm in diameter imaged in Fig. 1c. We used scanning impedance microscopy to verify that this structure was the only current path connecting source and drain contacts. For fixed V_g, the source–drain current data show the expected thermally activated dependence. We use an Arrhenius plot to extract an activation energy E_a (Fig. 4b, inset), which is plotted as a function of V_g in Fig. 3b.

The linear regions in Fig. 3b (-2 V $< V_g < 2$ V) occur when E_F is situated in the bandgap of the semiconducting SWNT. At $V_g = 0$, E_a reaches a maximum of about 150 meV; the energy gap of this SWNT is therefore 300 meV, corresponding to a nanotube diameter near 2 nm that is compatible with that of the AFM images of the structure (Fig. 1c). From a linear fit to E_a in the gap region, the ratio of gate capacitance to total capacitance, or 'lever arm', is found to be $\alpha \approx 0.08$, similar to the value of 0.1 found for CVD-grown samples with the same device geometry[8]. The activation energy oscillates for $-8\ \text{V} < V_g < -2\ \text{V}$ as does $I(V_g)$. We attribute these oscillations to single-electron charging and note that a maximum (minimum) in the activation energy near $V_g = -6$ V ($V_g = -8$ V, -4 V) corresponds to a minimum (maximum) in $I(V_g)$, as expected for the charging regime.

Figure 4a shows $I(V_g)$ data as a function of temperature for device II, a p-type FET. Again we observe that E_a increases linearly with gate voltage in the range $-4\ \text{V} < V_g < 0$ V, as expected within the model. We cannot determine E_a for positive V_g because the current at low temperature is below measurement sensitivity, but the data indicate an energy gap greater than 400 meV and a lever arm $\alpha \approx 0.03$. As is the case for device I, $I(V_g)$ and $E_a(V_g)$ exhibit oscillations that are attributed to Coulomb effects.

In conclusion, we have demonstrated significant progress towards the goal of fabricating SWNT nanoeletronic devices from bulk HiPCO-grown material. Devices fabricated from raw HiPCO have very high resistance; careful purification is thus essential for removing impurities that degrade device characteristics. After purification, resuspension, deposition, and surfactant removal, SWNTs retain the unique electronic properties that make them leading candidates for nanoelectronic devices. Finally, we demonstrate how the energy gap of individual semiconducting nanotubes can be quantitatively inferred from measurements of device current as a function of temperature and gate voltage.

METHODS

DETAILS OF THE PURIFICATION PROCESS

Wet air burn. Impurity carbon phases (amorphous carbon, fullerenes, etc.) were removed by heating raw HiPCO material in air in the presence of H_2O_2 for 3–6 h.

Acid treatment. Oxidized SWNT material was refluxed with 2–3 M HNO_3 for 20 min, neutralized with NaOH, and then washed with deionized water. The material was refluxed with H_2O_2 for 10 min. These two steps were repeated 2–3 times.

Annealing. The material was annealed in vacuum at 1,150 °C for 2–3 h.

Magnetic fractionation. SWNT material was dispersed in NaDDBS surfactant solution as detailed in ref. 11. The material was flowed over a magnetic field gradient ($\sim$0.08 T cm^{-1}). Magnetic impurities felt a force due to the field gradient and were removed from the main flow of material.

Received 7 February 2005; accepted 23 May 2005; published 17 July 2005.

References

1. McEuen, P. L. Single-wall carbon nanotubes. *Phys. World* **13**, 31–36 (2000).
2. Nikolaev, P. *et al.* Gas-phase catalytic growth of single-walled carbon nanotubes from carbon monoxide. *Chem. Phys. Lett.* **313**, 91–97 (1999).
3. Bronikowski, M. J., Willis, P. A., Colbert, D. T., Smith, K. A. & Smalley, R. E. Gas-phase production of carbon single-walled nanotubes from carbon monoxide via the HiPCO process: A parametric study. *J. Vac. Sci. Technol. A* **19**, 1800–1805 (2001).
4. Antonov, R. D. & Johnson, A. T. Subband population in a single-wall carbon nanotube diode. *Phys. Rev. Lett.* **83**, 3274–3276 (1999).
5. Hafner, J. H., Cheung, C. L. & Lieber, C. M. Direct growth of single-walled carbon nanotube scanning probe microscopy tips. *J. Am. Chem. Soc.* **121**, 9750–9751 (1999).
6. Freitag, M., Johnson, A. T., Kalinin, S. V. & Bonnell, D. A. Role of single defects in electronic transport through carbon nanotube field-effect transistors. *Phys. Rev. Lett.* **89**, 216801 (2002).
7. Javey, A., Qi, P. F., Wang, Q. & Dai, H. J. Ten- to 50-nm-long quasi-ballistic carbon nanotube devices obtained without complex lithography. *Proc. Natl Acad. Sci. USA* **101**, 13408–13410 (2004).
8. Radosavljevic, M., Freitag, M., Thadani, K. V. & Johnson, A. T. Nonvolatile molecular memory elements based on ambipolar nanotube field effect transistors. *Nano Lett.* **2**, 761–764 (2002).
9. Mann, D., Javey, A., Kong, J., Wang, Q. & Dai, H. J. Ballistic transport in metallic nanotubes with reliable Pd ohmic contacts. *Nano Lett.* **3**, 1541–1544 (2003).
10. Bachilo, S. M. *et al.* Narrow (n,m) distribution of single-walled carbon nanotubes grown using a solid supported catalyst. *J. Am. Chem. Soc.* **125**, 11186–11187 (2003).
11. Islam, M. F., Rojas, E., Bergey, D. M., Johnson, A. T. & Yodh, A. G. High weight fraction surfactant solubilization of single-wall carbon nanotubes in water. *Nano Lett.* **3**, 269–273 (2003).
12. Moore, V. C. *et al.* Individually suspended single-walled carbon nanotubes in various surfactants. *Nano Lett.* **3**, 1379–1382 (2003).
13. Zheng, M. *et al.* Structure-based carbon nanotube sorting by sequence-dependent DNA assembly. *Science* **302**, 1545–1548 (2003).
14. Zorbas, V. *et al.* Preparation and characterization of individual peptide-wrapped single-walled carbon nanotubes. *J. Am. Chem. Soc.* **126**, 7222–7227 (2004).
15. Liu, J. *et al.* Fullerene pipes. *Science* **280**, 1253–1256 (1998).
16. Doorn, S. K. *et al.* High resolution capillary electrophoresis of carbon nanotubes. *J. Am. Chem. Soc.* **124**, 3169–3174 (2002).
17. Krupke, R., Hennrich, F., Lohneysen, H. v. & Kappes, M. M. Separation of metallic from semiconducting single-walled carbon nanotubes. *Science* **301**, 344–347 (2003).
18. Strano, M. S. *et al.* Electronic structure control of single-walled carbon nanotube functionalization. *Science* **301**, 1519–1522 (2003).
19. Liu, J. *et al.* Controlled deposition of individual single-walled carbon nanotubes on chemically functionalized templates. *Chem. Phys. Lett.* **303**, 125–129 (1999).
20. Rao, S. G., Huang, L., Setyawan, W. & Hong, S. Large-scale assembly of carbon nanotubes. *Nature* **425**, 36–37 (2003).
21. Islam, M. F., Milkie, D. E., Kane, C. L., Yodh, A. G. & Kikkawa, J. M. Direct measurement of the polarized optical absorption cross section of single-wall carbon nanotubes. *Phys. Rev. Lett.* **93**, 037404 (2004).
22. Islam, M. F., Milkie, D. E., Torrens, O. N., Yodh, A. G. & Kikkawa, J. M. Magnetic heterogeneity and alignment of single wall carbon nanotubes. *Phys. Rev. B* **71**, 201401 (2005).
23. Radosavljevic, M., Lefebvre, J. & Johnson, A. T. High-field electrical transport and breakdown in bundles of single-wall carbon nanotubes. *Phys. Rev. B* **64**, 241307 (2001).
24. Freitag, M., Radosavljevic, M., Zhou, Y. X., Johnson, A. T. & Smith, W. F. Controlled creation of a carbon nanotube diode by a scanned gate. *Appl. Phys. Lett.* **79**, 3326–3328 (2001).
25. Appenzeller, J. *et al.* Field-modulated carrier transport in carbon nanotube transistors. *Phys. Rev. Lett.* **89**, 126801 (2002).
26. Durkop, T., Getty, S. A., Cobas, E. & Fuhrer, M. S. Extraordinary mobility in semiconducting carbon nanotubes. *Nano Lett.* **4**, 35–39 (2004).
27. Heinze, S., Tersoff, J. & Avouris, P. Electrostatic engineering of nanotube transistors for improved performance. *Appl. Phys. Lett.* **83**, 5038–5040 (2003).

Acknowledgements

A.G.Y. acknowledges partial support from NSF DMR-0203378 and NASA (NAG8-2172).
D.E.J. acknowledges support from NSF IGERT (DGE-0221664). A.G.Y. and A.T.J. acknowledge support from NSF MRSEC DMR-079909. A.T.J. acknowledges partial support from the Petroleum Research Fund.
Correspondence and requests for materials should be addressed to M.F.I. or A.T.J.
Supplementary Information accompanies this paper on www.nature.com/naturematerials.

Competing financial interests

The authors declare that they have no competing financial interests.